energy&fuels

pubs.acs.org/EF Article

Characterization of Activated Carbons Prepared from Almond Shells and Their Hydrogen Storage Properties

Zeynep Bicil and Mehmet Doğan*

Cite This: *Energy Fuels* 2021, 35, 10227−10240 Read Online

ACCESS | Metrics & More | Article Recommendations

ABSTRACT: In this study, activated carbons with a well-developed porous structure and high surface area were prepared from almond shells by chemical activation using zinc chloride and microwave irradiation methods under a nitrogen atmosphere. The effects of microwave irradiation times, powers, agent ratios on pore volumes, and BET surface areas of the activated carbons were investigated. Pore volumes and BET surface areas of the activated carbons were determined using a BET surface area device; surface functional groups using an FTIR-ATR spectroscope; surface morphology using an SEM/EDX device; and hydrogen storage capacities using an IMI PSI gas storage device. Both the BET surface areas and total pore volumes of activated carbons with increasing microwave irradiation time, power, and agent ratio increased. Experimental studies showed that AC600 with the highest BET surface area (1307 m^2/g) and total pore volume (1.66 cc/g) had the highest hydrogen storage capacity (2.53 wt %) at 77 K. FTIR-ATR and SEM analyses indicated that the morphology of the almond shell changed with $ZnCl_2$ activation and the microwave process and it transformed into a carbon-like structure. The hydrogen storage capacity of activated carbons at cryogenic temperature was higher than that at room temperature. The adsorption data were correlated reasonably well by Freundlich adsorption isotherms.

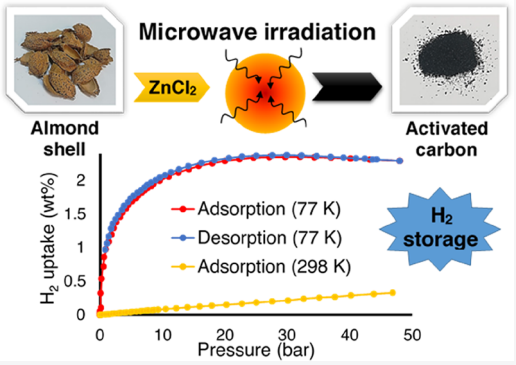

1. INTRODUCTION

In our age, when energy has become the most important need for us to sustain our existing lives, the increasing population increases this demand for energy even more. Most of the world's energy demand is supplied from hydrocarbon-based fossil sources such as coal, crude oil, and natural gas. However, these fossil sources decrease in time and gases such as CO_2, SO_2, and NO_x released as a result of combustion of these sources cause significant air pollution, acid rain, and greenhouse effect.[1] Energy sources, which will be an alternative to fossil fuels, should have features such as environment-friendly, high reserve, renewable, carbonless structure, and high energy content. Hydrogen having these properties is called the fuel of the future and stands out as the most important alternative energy carrier to replace fossil fuel systems at the end of the 21st century. In addition, hydrogen, which has higher chemical energy than hydrocarbon fuels, can be easily produced with different techniques without emission of pollutants or greenhouse gases.[2−4] The most important property of hydrogen is that it can be stored, but because hydrogen is the lightest fuel, its storage is a major problem. Several methods such as high-pressure hydrogen, liquid hydrogen, physisorption, and chemisorption have been proposed.[5,6] Hydrogen embrittlement occurs in the structures of the tanks at high pressures. This may cause corrosion in the structure of the tank. The result is a dangerous situation.[7,8] At the same time, storage in gas and liquid phases requires both large volumes and high costs. Therefore, for practical applications, hydrogen must be stored efficiently, safely, and cheaply.[2] Today, studies focus on either improving present technologies or advanced materials. The methods such as storage in glass spheres,[9] storage in caves,[10] separation from hydrocarbons,[11] and use of metal hydride[12] have been developed. Another storage method is hydrogen adsorption on carbon-based materials. This method is based on the storage of hydrogen under pressure on the surface of porous carbon-based materials. Due to their reliability and their ability to store high amounts of hydrogen, a great number of studies on activated carbons,[2] carbon nanofibers,[13] carbon nanospheres,[14] and carbon nanotubes[7] have been carried out in recent years.

Activated carbon from these adsorbents is defined as a carbonaceous adsorbent with a very large internal surface area.[15] Today, activated carbon is obtained in one or two steps

Received: March 14, 2021
Revised: May 11, 2021
Published: May 25, 2021

https://doi.org/10.1021/acs.energyfuels.1c00795
Energy Fuels 2021, 35, 10227−10240

by physical or chemical activation methods from carbon-based fossil sources or renewable biomass. In the generally two-step physical activation, precursor materials are first carbonized under an inert atmosphere. Then, the activation of the carbonized material is carried out at high temperatures in the presence of oxidizing gases such as steam, CO, and CO_2. Although it is considered as an ecological approach because it does not contain chemicals, physical activation has disadvantages such as low adsorption capacity and high energy consumption. In chemical activation, carbonization and activation are generally carried out simultaneously. This saves time and energy, which is a good advantage against physical activation.[16] The common feature of these two methods is that the material is heated to a high temperature. At this stage, conventional heating is used for decades, and the material has been heated by conduction or convection, so there is a temperature fluctuation from the surface of the particles to the interior. As a result, gaseous byproducts cannot be removed effectively.[17] A new method is the microwave irradiation method. In this method, materials receive energy through dipole rotation and ionic conduction. A homogeneous warming occurs in the particles, and a temperature gradient does not occur. In conventional heating, the furnace and interior walls must first heat up, which leads to serious waste of time and energy.[18] For these reasons, microwave energy has been recently used in the preparation of activated carbon from different materials such as coals, peanut hulls, coconut shells, cotton stalks, bamboos, waste teas, orange peels, coffee shells, and corn cobs.[19−27]

In the literature, activated carbons were prepared from different biomasses by physical and chemical methods and the hydrogen storage capacities of some of them were determined.[28,29] There is an increase in the number of studies aimed at determining the hydrogen storage capacity of activated carbons prepared by the microwave irradiation method. For example, Li et al. (2016) prepared the activated carbon with a 3149 m^2/g surface area from carbonized materials and reported that activated carbon with the highest hydrogen storage capacity (0.91 wt %) was produced in 9 min with 800 W radiation.[26] Ramesh et al. (2015) studied the hydrogen adsorption behavior of activated carbons derived from tamarind seeds and found that the hydrogen storage capacity of activated carbon with a 1785 m^2/g surface area was 4.73 wt % at room temperature and 40 bar.[30] Activated carbons were produced from almond shells by physical and chemical activation methods.[31−33] Izgi et al. (2019) prepared activated carbon by microwave irradiation from almond shells and determined that the maximal surface area was 1128 m^2/g;[34] and Du et al. (2016) studied the synthesis of a novel adsorbent from waste almond shells (AS) and found that the optimized activated carbon preparation conditions were to be as follows: a mass ($ZnCl_2$/AS) ratio of 3:1 (w/w) and microwave heating time period of 15 min at 900 W.[35] As can be seen from the above studies, there is no study on the production of activated carbon from almond shells by the microwave irradiation method to store hydrogen. Furthermore, almond shells are an agricultural waste like biomasses used in the production of some other activated carbon. The utilization of agricultural wastes and bringing them into the economy are procedures that are possible with activated carbon production. Therefore, the aims of the study are to prepare the activated carbons under different conditions from almond shells using the microwave irradiation method; to optimize the prepared activated carbons according to their specific surface areas and pore volumes; to characterize with FTIR-ATR and SEM/EDX instruments; and, for the first time, to measure the hydrogen adsorption capacities of the activated carbons at room and cryogenic temperatures. The novelty of this study is to bring the almond shell, which is an agricultural waste, to the economy, to produce activated carbon by $ZnCl_2$ activation using the microwave method, and to use the produced activated carbon for hydrogen storage for the first time.

2. MATERIALS AND METHODS

2.1. Materials. Almond shells used as raw biomass were obtained from Balikesir in Turkey. The $ZnCl_2$ and HCl chemicals used in the study were purchased from Merck-Sigma Aldrich and had purities of 98 and 37%, respectively.

2.2. Preparation of Activated Carbons. Almond shells were washed with plenty of distilled water to remove dust on them, dried at 105 °C for 1 day in an oven, ground using a Waring blender, and sieved with a Retsch AS200 vibrating siever to obtain particles in a particle size range of 100−500 μm. Samples for chemical activation of almond shells were treated with $ZnCl_2$ (1:4, almond shell:agent) for 23 h at room temperature and 1 h at an ultrasonic bath. Then, they were subjected to microwave irradiation for different times (15, 30, 45, and 60 min) at 350 W. The resulting activated carbon was first treated with 0.1 M hydrochloric acid solution and then washed with hot water and water until the pH was 6−7. The washed samples were dried in an oven at 105 °C. In this way, the effect of time on the surface areas of activated carbons was determined and the BET surface areas and pore volumes of the samples were measured. For the optimization of the time, the sample with the highest surface area was selected. Subsequent studies were carried out to investigate the effect of almond shell:agent ratio on the surface area of activated carbon in a fixed time. The experimental processes above were applied for the other parameters. After determining the effect of time and almond shell:agent ratio on the BET surface areas of activated carbons, the effect of microwave irradiation power was investigated. The flow diagram used in activated carbon production is given in Figure 1. In the synthesis of activated carbon, 1.3 g of AC600 sample was produced from 5 g of almond shells.

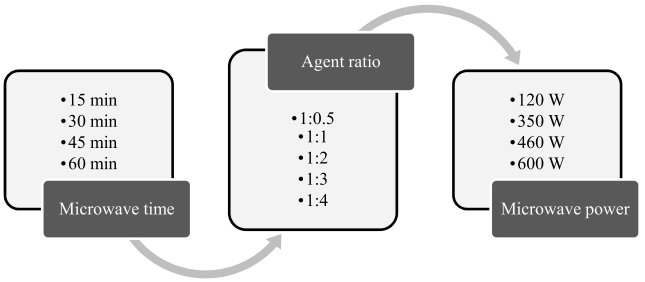

Figure 1. Optimization scheme used to prepare activated carbon from almond shells.

2.3. Characterization of Activated Carbons. BET surface areas of activated carbons were measured by using pure nitrogen gas in liquid nitrogen with a Quantachrome Nova 2200e series device at 77 K. The samples were degassed at 250 °C for 24 h before BET analysis. The specific surface area (S_{BET}) was obtained by the BET method using adsorption data in the 0.05−0.3 relative pressure range. Micropore volume (V_{DA}) was determined using the Dubinin−Astakhov (DA) method. Total pore volume was calculated using the amount of N_2 adsorbed at a 0.99 relative pressure. Volumes and size distributions of pores with a width of 0−40 nm were calculated from the density functional theory (DFT) method (slit pore, NLDFT equilibrium model). The mesopore volume was calculated by subtracting the micropore volume (calculated by the DA method) from the pore volume obtained by the DFT method. TG

https://doi.org/10.1021/acs.energyfuels.1c00795
Energy Fuels 2021, 35, 10227−10240

thermograms of the samples were performed between room temperature and 600 °C under a nitrogen atmosphere at heat rates of 10 °C per minute using a PerkinElmer Diamond DTA/TG device. The surface morphology of the samples was studied with a scanning electron microscope (SEM, Zeiss EVO LS 10). In addition, the percentage of carbon and oxygen contained in the samples was calculated by using the EDX probe. The Fourier transform infrared spectra of activated carbons were obtained with a PerkinElmer Spectrometer 100 device in a wavelength range of 4000−600 cm^{-1}.

2.4. Electrokinetic Properties. Electrokinetic measurements were performed using the Malvern ZetasizerNanoS device. The zeta potential measurements were carried out as a function of initial solution pH. In the experiments, 1 g of activated carbon was transferred into a 250 mL polyethylene bottle and 100 mL of water was put on it. The activated carbons were dispersed using a thermostated shaker bath. The pH was measured with an Orion 920A pH meter and adjusted by HCl or NaOH solutions. After shaking for 24 h, the suspension samples taken from the supernatant were placed in the measuring cell and then their zeta potentials were measured.[36,37]

2.5. Hydrogen Adsorption Experiments. The hydrogen adsorption capacities of all samples were determined at room and cryogenic temperatures as a function of pressure. The hydrogen storage capacities of the activated carbons were measured with a Hiden IMI PSI gas storage device. Before the analysis, samples were degassed at 250 °C for 24 h.[2,7]

3. RESULTS AND DISCUSSION

3.1. Characterization. *3.1.1. Optimization of Microwave Irradition Time.* The heating time in the preparation of conventional activated carbons is approximately 2 h. In this process, heat is transferred from the surface into the particle. Particle size and shape for heat transfer are very important. As the particle size increases, the temperature gradient within the particle also increases.[38] Irregularly shaped activated carbons may have non-uniform temperature distribution within the furnace. This situation may cause some points of the activated carbon to burn, which affects the uniformity of activated carbon surface properties and pore structure development.[17] Since one of the aims of this study was to obtain activated carbon using less energy, the microwave irradiation time was tried to be kept as short as possible. One of the important parameters affecting the activation degree of activated carbons is the microwave irradiation time.[39,40] In the microwave process, heat transfer occurs by a different mechanism compared to conventional heating, resulting in the unique properties of microwave heating. The microwave absorption capacity of the activated carbon precursor is more important than particle size and shape and volumetric properties of microwave heating. Since the moisture in the structure of a sample will consume more energy, the heating rate for convectional activation decreases.[17] For this reason, four different times were chosen, namely, 15, 30, 45, and 60 min. When the microwave irradiation time increases, more energy is transferred to the activated carbon precursor and the temperature of the sample becomes higher even if the microwave power is set at the same level. When microwave irradiation time is longer, much more active sites and pores are initially formed on the surface of samples.[17] Almond shells with a particle size of 100−500 μm were activated at a ratio of 1:4 (almond shell:agent) using $ZnCl_2$ for 24 h. These activated materials were subjected to microwave energy at a 350 W irradiation power under a N_2 atmosphere for the times mentioned above. These samples obtained were washed with distilled water and dried at 105 °C in an oven for 24 h, and then, their BET surface areas and pore volumes were measured. The variation of the BET surface areas and pore volumes of the prepared activated carbon samples with the microwave irradiation time is given in Figure 2a. As seen in

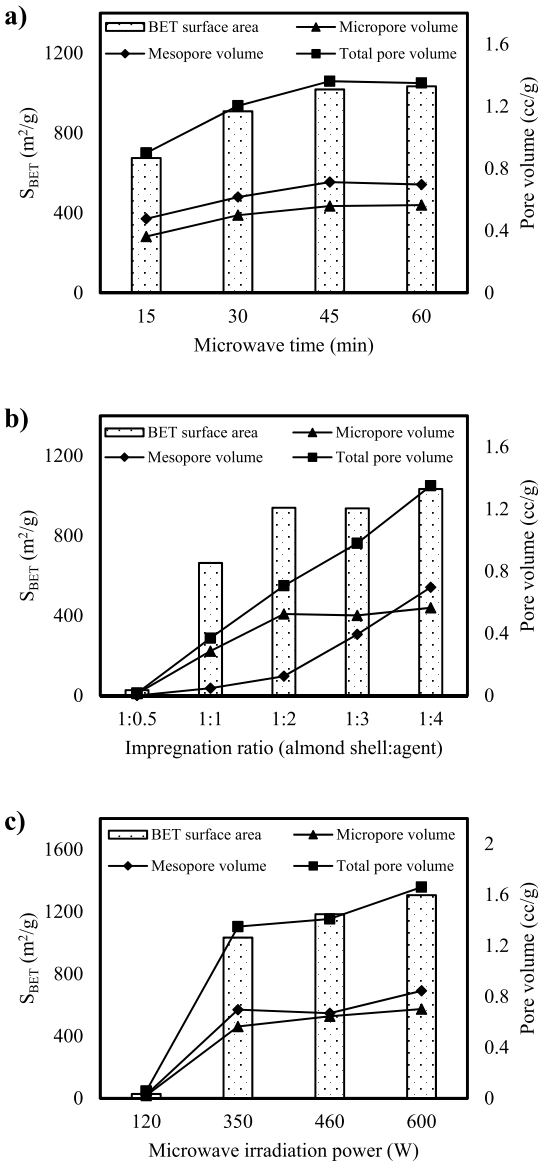

Figure 2. Effect of (a) microwave irradiation time, (b) agent ratio, and (c) microwave irradiation power on the textural properties of activated carbons.

Figure 2a, the surface areas, micropore volumes, mesopore volumes, and total pore volumes of activated carbon samples increased with increasing microwave irradiation times. This case shows that more active sites and pores with increasing time are formed in the sample. Table 1 shows EDX analysis of activated carbon samples. As the microwave irradiation time increases, the carbon content increases while the oxygen content decreases. This result shows that as the microwave irradiation time increases, more volatile components will move away from the structure. Thus, it can be said that the microwave process has a significant effect on the surface properties of activated carbons as it eliminates oxygen-containing functional groups and increases the carbon/oxygen ratio.[38] In addition, it was observed that micro- and mesopore

https://doi.org/10.1021/acs.energyfuels.1c00795
Energy Fuels 2021, 35, 10227−10240

Table 1. Preparation Conditions, Textural Property Values, and Carbon and Oxygen Contents of Activated Carbons Prepared from Almond Shells and Their Hydrogen Storage Capacities at Different Temperatures

samples	MW time (min)	agent ratio (almond shell:agent)	MW power (W)	S_{BET} (m^2/-g)[a]	V_t (cc/g)[b]	V_{mic} (cc/g)[c]	V_{DFT} (cc/g)[d]	V_{meso} (cc/g)[e]	H_2 uptake % at 77 K (27 bar)	H_2 uptake % at 298 K (47 bar)	C (wt %)	O (wt %)
AC15	15	1:4	350	675	0.900	0.363	0.840	0.477	1.37	0.17	71.4	27.8
AC30	30	1:4	350	909	1.204	0.500	1.117	0.617	1.66	0.22	89.3	6.5
AC45	45	1:4	350	1018	1.362	0.559	1.272	0.713	2.04	0.22	92.5	6.4
AC60	60	1:4	350	1034	1.350	0.565	1.262	0.697	2.34	0.27	93.3	5.5
AC105	60	1:0.5	350	27	0.016	0.012	0.013	0.001	0.20	0.10	57.6	40.5
AC11	60	1:1	350	664	0.370	0.286	0.334	0.048	1.41	0.31	91.9	6.3
AC12	60	1:2	350	940	0.707	0.525	0.650	0.125	2.03	0.20	93.8	5.1
AC13	60	1:3	350	937	0.980	0.516	0.910	0.394	1.87	0.28	93.1	6.2
AC120	60	1:4	120	28	0.056	0.022	0.050	0.028	0.27	0.10	71.5	28.1
AC460	60	1:4	460	1185	1.410	0.645	1.314	0.669	2.35	0.21	94.4	4.8
AC600	60	1:4	600	1307	1.661	0.702	1.547	0.845	2.53	0.22	98.8	1.1

[a]S_{BET}, calculated by BET equation at P/P_0 = 0.05−0.3. [b]V_t, estimated from the adsorption amount of N_2 at P/P_0 = 0.99. [c]V_{mic}, calculated by the DA method. [d]V_{DFT}, calculated by the DFT method using a slit pore model. [e]It was obtained by subtracting the micropore volume from the pore volume calculated by the DFT method.

volumes were approximatelly formed equally. Similar trends were seen in the production of activated carbon from bamboo.[23] As a result of microwave irradiation time, the optimal time was determined as 60 min. Under these conditions, the BET surface area of the activated carbon was 1034 m^2/g.

3.1.2. Optimization of Agent Ratio. The decrease in (biomass:agent) ratio in chemical activation positively affects the activation up to the optimum impregnation ratio. Since further increasing in the reagent ratio will cause burning and blocking the pores, it negatively affects the surface properties of the activated carbon. Hence, the accessible area reduces.[38] In this study, five different ratios were chosen to examine the agent effect, namely, 1:0.5, 1:1, 1:2, 1:3, and 1:4 (almond shell:$ZnCl_2$, w:w). Certain amounts of the sieved and dried almond shells were mixed with the agent for 24 h at room temperature. The samples were then subjected to microwave irradiation at a power of 350 W under a N_2 atmosphere for 60 min. In Figure 2b, the surface areas of the samples increased with the decrease in the impregnation mass ratio from 1:0.5 to 1:4. The reason for the increase is that the increased amount of $ZnCl_2$ suppresses tar formation and facilitates the release of volatile components.[41] The BET surface area of the activated carbon produced in a mass ratio of 1:4 (biomass:agent) is 1034 m^2/g. Again, from Figure 2b, it is seen that the total pore volume increases linearly with increasing agent ratio, that more micropores form at a 1:2 ratio, and after that point, that the mesopores begin to form at a high ratio. The BET surface area results obtained show a similar trend to the surface area results prepared with different $ZnCl_2$ ratios from the pistachio shell.[41] Based on the BET surface area and total pore volume, the optimum agent ratio for the next experimental study was selected as 1:4.

3.1.3. Optimization of Microwave Irradiation Power. Four different values (120, 350, 460, and 600 W) were studied for optimization of microwave irradiation powers. The ground and sieved almond shells were treated with a 1:4 almond shell:$ZnCl_2$ agent ratio. They were then exposed to microwave irradiation under a N_2 atmosphere for 60 min at the specified powers. High microwave irradiation power provides more energy to the sample, which causes more active sites and pore formation on the sample.[17] It is understood from Figure 2c that as the irradiation power increases, the surface area and the total pore volume increase significantly. By looking at the ratio of meso- and micropores to total pore volume, it can be said that the amount of the forming mesopores increases as the power increases. It is clearly stated in the literature that after the microwave power exceeds a certain level, excess energy burns a small amount of carbon and the pore structure is destroyed.[22] For this reason, higher microwave irradiation power was not tested in this study.

3.2. FTIR Spectra of Activated Carbons. The FTIR spectra of the activated carbons and almond shells are given in Figure 3. Spectra were arranged according to three parameters whose optimization was studied, and each group was compared with the spectrum of almond shells. The broad peak at around 3334 cm^{-1} in the FTIR spectrum of the almond shell is a classical O−H peak belonging to the hydroxyl group. The double peaks at around 2917 cm^{-1} arise from the stretching vibrations of the C−H bond in the methyl and methylene groups. Peaks at around 1741 and 1032 cm^{-1} indicate the presence of the carbonyl group and the C−O bond, respectively. The peak at around 1570 cm^{-1} in the spectrum of the activated carbons belongs to the stretching vibrations of the C═C double bond. The sharp peak at 1032 cm^{-1} in the spectrum of almond shells becomes broader in the activated carbon spectra and is related to the C−O bond of various functional groups.[23] As shown in Figure 3a, as the microwave irradiation time increases, the peak intensity of the C═C double bond increases and this peak becomes more pronounced. This means that as the irradiation time gets longer, the amount of carbon in the structure increases. The spectra in Figure 3b show that the agent ratio and the carbonization ratio are directly proportional. As the agent ratio increases, the intensity of the activated carbon peaks mentioned above also increases. When the spectrum of activated carbon prepared at 120 W microwave irradiation power is examined (Figure 3c), it is seen that the carbonization is not completed and there are still peaks of almond shells.

3.3. SEM/EDX Images of Activated Carbons. Table 1 shows the amount of carbon and oxygen of the prepared activated carbons. As the microwave irradiation time, power, and agent ratio increase, the carbon content of the activated carbon increases. The high carbon ratio indicates that the carbonization process is successful. The SEM images in Figure 4 show that AC15 has less porosity than other activated carbon

https://doi.org/10.1021/acs.energyfuels.1c00795
Energy Fuels 2021, 35, 10227−10240

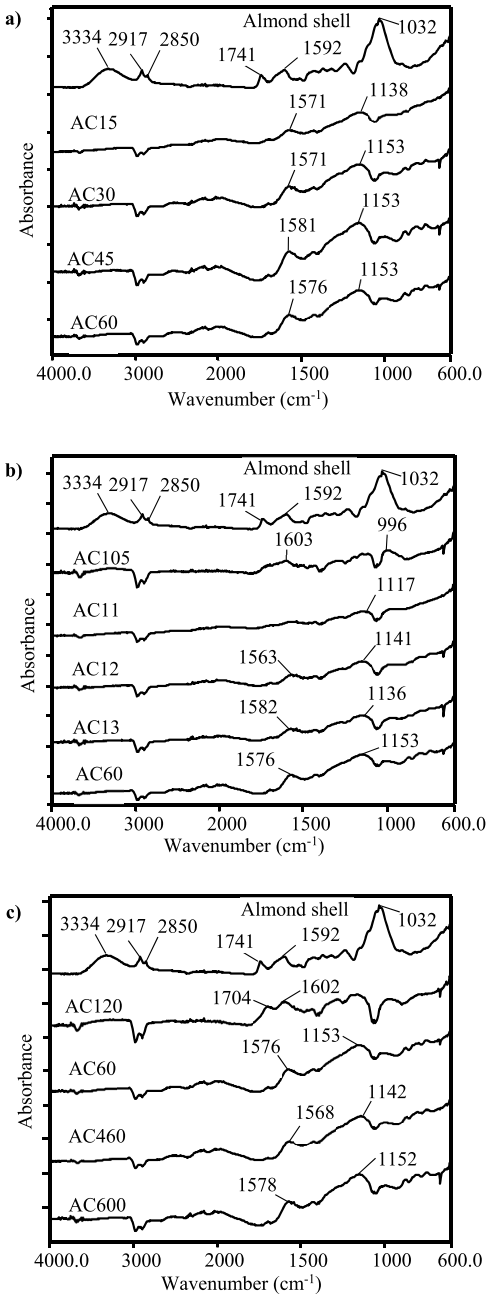

Figure 3. FTIR-ATR spectra of activated carbon samples prepared using different (a) microwave times, (b) agent ratios, and (c) microwave irradition powers.

samples. Moreover, the fact that the carbon content of AC15 is 71.4 wt % indicates that the time for both carbonization and pore formation is insufficient. It is clear that AC105, which has the least carbon content among the activated carbons prepared in Figure 5, has a nonporous structure compared to the others. According to the images, it is possible to say that the higher the agent ratio, the higher the pore formation. In the SEM image of AC120 prepared in the lowest microwave irradiation power (Figure 6), it is seen that the pore formation is not completed. EDX patterns showing the change in carbon and oxygen contents depending on the increase in surface areas of some activated carbons are given in Figure 7. Depending on the increase in the surface area, the carbon content of the samples also increases.

3.4. TG Thermograms of Almond Shells and AC600. TG thermograms of both the almond shell and the AC600 sample were taken to compare the thermal stability of the almond shell and activated carbons. TG analysis gives important information both about the maximum decomposition temperatures of the biomasses and the mass losses at these decomposition temperatures. These decomposition temperatures are explained depending on the chemical components of the biomass, the chemical bond structure, and the catalytic effect of the ash and/or inorganic residue. In this study, TG thermograms of both the almond shell and the AC600 sample with the highest micropore volume area were taken with temperature increases of 10 °C per minute between room temperature and 600 °C under a nitrogen atmosphere. Figure 8 shows the TG thermograms of the almond shell and AC600 sample. While the almond shell degrades in two steps, the AC600 sample is thermally very stable. The firs mass loss (4.06 wt %) between 38 and 90 °C of the almond shell is due to the removal of moisture from the structure. The second mass loss (70.05 wt %) between 209 and 425 °C can be attributed to the degradation of cellulose, hemicellulose, and lignin in the structure and the removal of gaseous products and volatile components from the structure during decomposition.[2,42] For the almond shell, the total mass loss is 74.90 wt %. The total mass loss of the AC600 sample is 6.64 wt %. These results show that thermally highly stable activated carbons are produced.

3.5. Electrokinetic Properties. Figure 9 shows the change in zeta potential of activated carbon suspensions with initial solution pH. It is observed that the activated carbon samples have higher negative zeta potential at higher pH values, the negative value of zeta potential decreases with decreasing pH value, and zeta potential changes sign in a pH range of 3−4 and turns positive. It can be seen from Figure 9 that the activated carbon sample has an isoelectric point at pH = 3.7. This is very important in removing positively or negatively charged wastes from aqueous solutions. If the waste has a negative charge, adsorption experiments should be performed at low pH, or if it has a positive charge at low pH, adsorption experiments should be performed at high pH.

3.6. Hydrogen Storage. The amount of hydrogen that can be stored in an adsorption process is determined by the nature of the adsorbent and the operating conditions of the storage system.[43] Activated carbons have a wide area of research as gas storage materials because they are easily prepared compared to nanostructured carbons.[44] Activated carbon consisting of hydrophobic and hydrophilic sites is a carbon-based material with an amorphous and highly porous structure. Hydrophobic graphene planes are of great importance in the adsorption of neutral species and hydrophilic oxygen functional groups.[2] The hydrogen storage capacities of activated carbons produced from almond shells under different conditions in this study were measured at different temperatures and pressures, and the results have been discussed below.

3.6.1. Hydrogen Storage at Room Temperature. The hydrogen adsorption capacity of an adsorbent from gravimetric removal expressed as wt % can be calculated using eq 1

$$\text{wt \%} = \frac{m_{H_2}}{(m_{H_2} + m_s)} \times 100 \quad (1)$$

https://doi.org/10.1021/acs.energyfuels.1c00795
Energy Fuels 2021, 35, 10227−10240

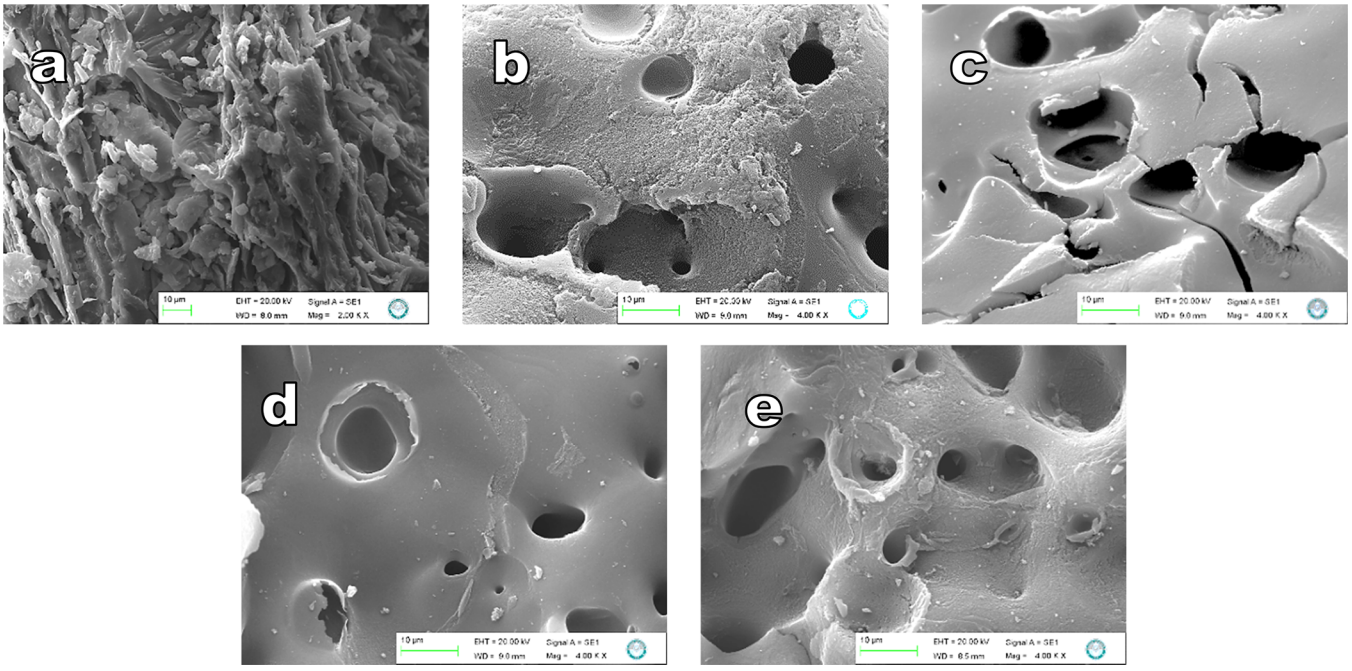

Figure 4. SEM images of (a) almond shell and activated carbon samples prepared at different microwave irradiation times: (b) 15 min, (c) 30 min, (d) 45 min, and (e) 60 min.

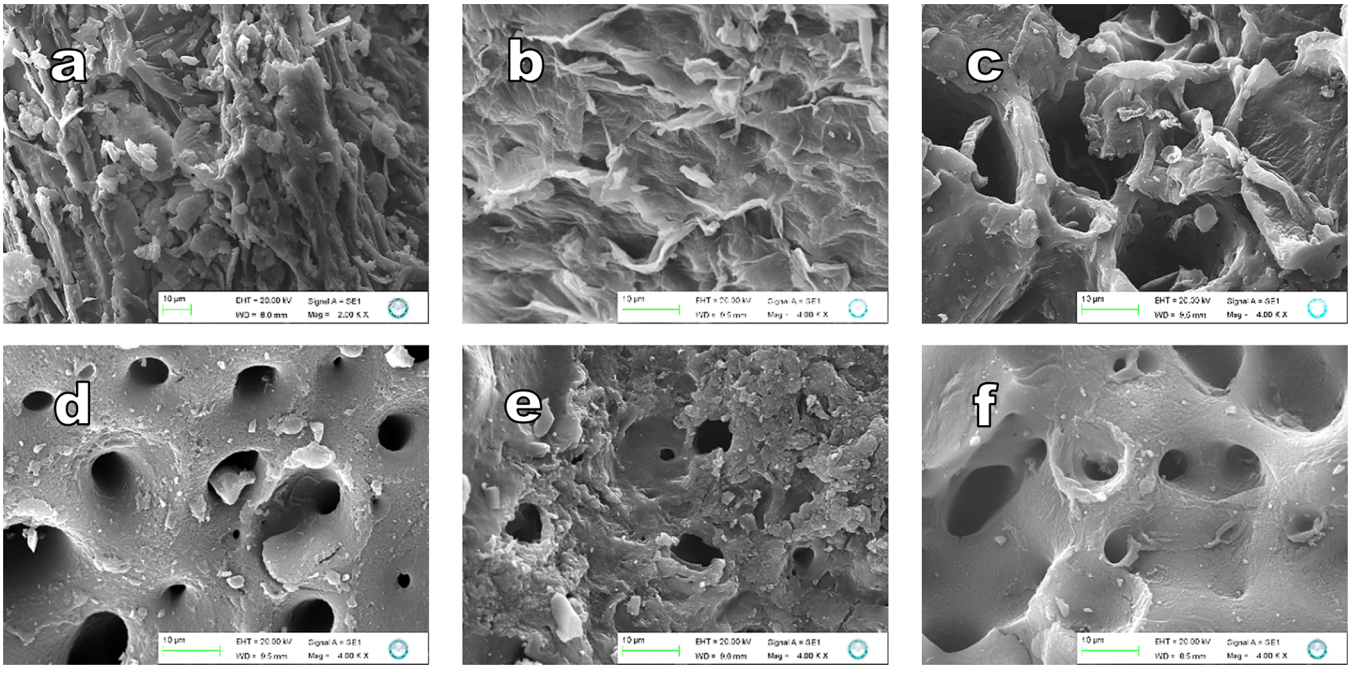

Figure 5. SEM images of (a) almond shell and activated carbon samples prepared at different agent ratios (almond shell:agent): (b) 1:0.5, (c) 1:1, (d) 1:2, (e) 1:3, and (f) 1:4.

where m_s is the mass of adsorbent and m_{H_2} is the mass of the adsorbed hydrogen. Figure 10a–c illustrates the hydrogen adsorption isotherms measured at room temperature of activated carbons produced at different microwave irradiation times, almond shell:agent ratios, and microwave irradiation powers with $ZnCl_2$ activation. These isotherms show that the H_2 uptake capacities of activated carbons increase with pressure. From isotherm curves, the maximum hydrogen storage capacities of the activated carbons produced with increasing microwave irradiation times such as 15 (0.17), 30 (0.22), 45 (0.22) and 60 (0.27) mins/wt % were measured; those with decreasing almond shell:agent ratios such as 1:0.5 (0.10), 1:1 (0.31), 1:2 (0.20), 1:3 (0.28), and 1:4 (0.27) as wt %; and those with increasing microwave irradiation powers such as 120 (0.10), 350 (0.27), 460 (0.21), and 600 (0.22) W/wt %, respectively. It was determined that the BET surface areas and total pore volumes of activated carbons produced by increasing microwave irradiation times, powers, and agent:almond shell ratios generally increased. In parallel with the BET surface area and pore volume measurements, the hydrogen

https://doi.org/10.1021/acs.energyfuels.1c00795
Energy Fuels 2021, 35, 10227−10240

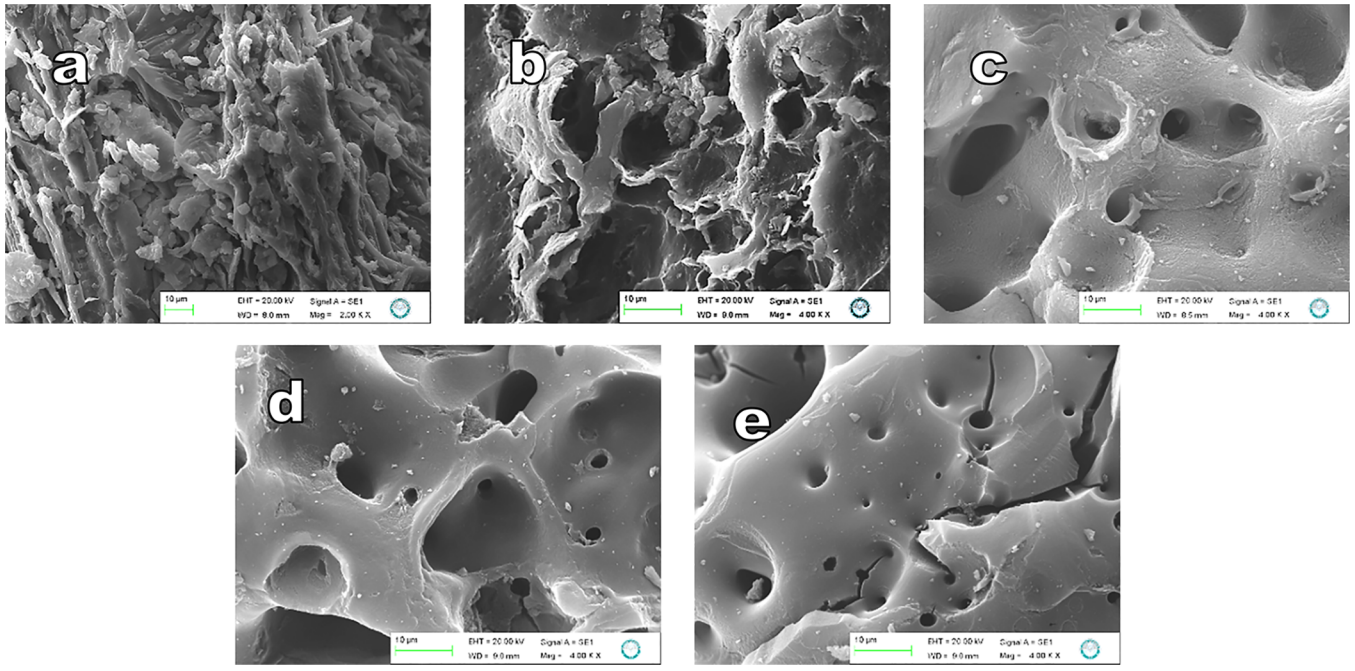

Figure 6. SEM images of (a) almond shell and activated carbon samples prepared at different microwave irradiation powers: (b) 120 W, (c) 350 W, (d) 460 W, and (e) 600 W.

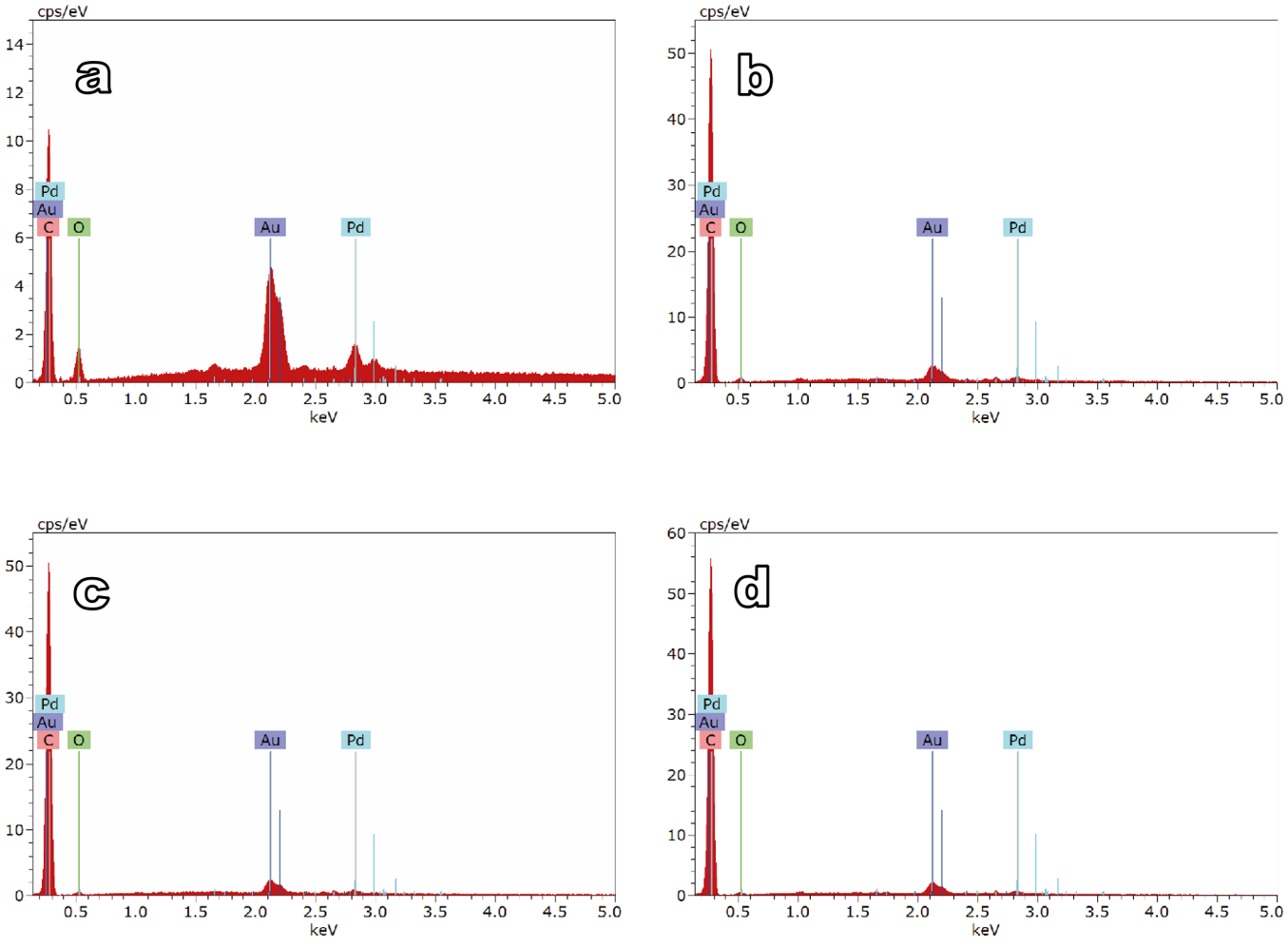

Figure 7. EDX patterns of some activated carbon samples: (a) AC120, (b) AC60, (c) AC460, and (d) AC600.

https://doi.org/10.1021/acs.energyfuels.1c00795
Energy Fuels 2021, 35, 10227−10240

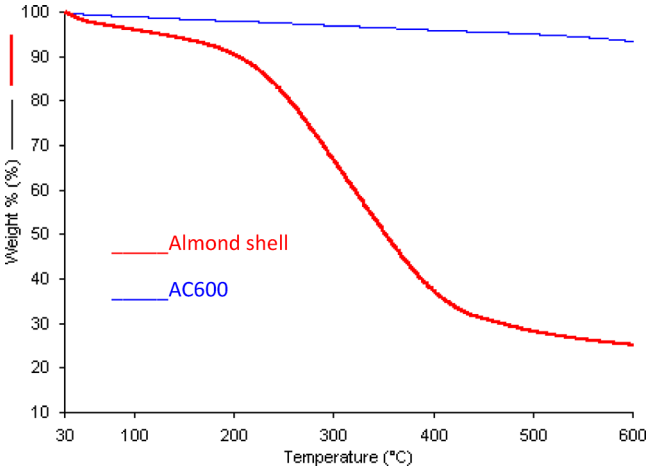

Figure 8. TG thermograms of the almond shell and AC600 sample.

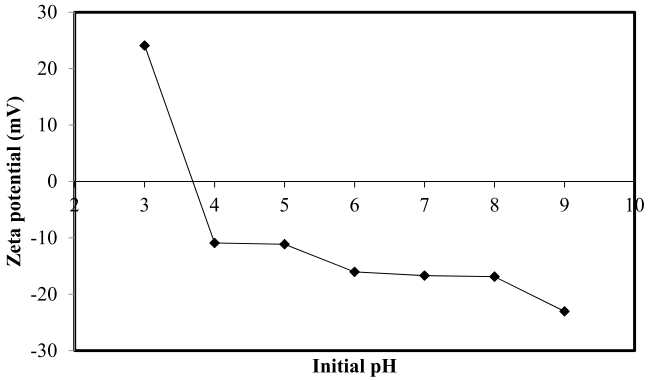

Figure 9. Variation of zeta potential with initial solution pH for AC600.

storage capacities of activated carbon samples also increased. In other words, as the microwave irradiation time, agent:almond shell ratio, and microwave irradiation power increased, the hydrogen storage capacities of the produced activated carbons also rose. The reason for this increase is the increase in the BET surface areas of activated carbons and especially the micropore volume, which is important in hydrogen adsorption. Again, it is seen that hydrogen adsorption isotherms do not reach saturation at room temperature and exhibit a linear relationship conforming to Henry's law. In this case, it can be said that only fractional coverage occurs and the adsorbed molecules behave like an ideal two-dimensional gas.[28] Different types of interactions may occur between the adsorbed hydrogen molecules and the adsorbent in the adsorption process of adsorbents with different pore volumes and surface areas. For example, hydrogen molecules for carbon-based adsorbents can be bonded to carbon atoms by covalent bonds. All carbon atoms attached to the three carbon atoms that hybridize to sp^2 have an idle π-bond. Therefore, carbon atoms can form chemical bonds with the hydrogen molecule.[45] The activation energy required for the physical adsorption of hydrogen is much lower than that for chemical adsorption.[46] Therefore, the possibility of chemical adsorption is very weak. In addition, high temperatures are also required for desorption of the adsorbed hydrogen in the case of chemical adsorption.[45] Theoretical studies show that the chemical adsorption probability of hydrogen at room temperature and atmospheric

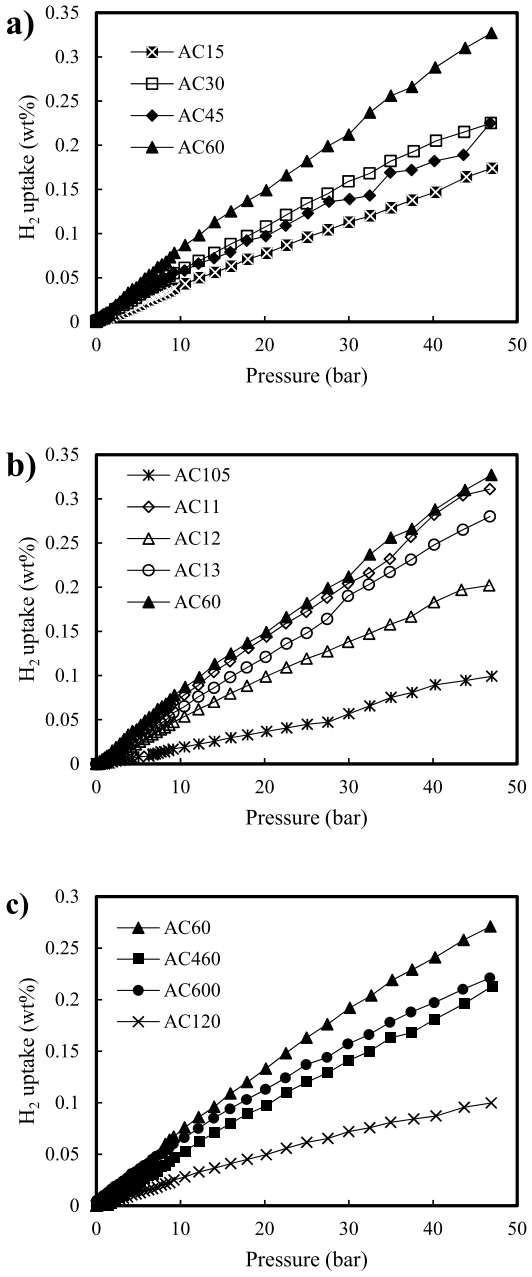

Figure 10. Hydrogen adsorption isotherms of activated carbons at 298 K (a) in different microwave times, (b) in different agent ratios, and (c) in different microwave irradition powers.

pressure is rather weak.[47] Thus, it can be said that no chemical interaction will occur between hydrogen and activated carbon. Generally, it is desired that hydrogen molecules interact with the adsorbent surface by reversible physical forces. Physical adsorption is a type of adsorption where hydrogen molecules are attached to the adsorbent surface by weak van der Waals interactions and the adsorption energy is around 20 kJ/mol. In this type of adsorption, hydrogen molecules preserve their molecular forms and do not participate in any chemical reaction. Therefore, physical adsorption is very fast and completely reversible.[48] At room temperature, Kojima et al. (2006) explained that the interaction between hydrogen and activated carbons based on the van der Waals force was the same order as the thermal motion energy of the hydrogen molecules on the surface.[43] The hydrogen storage capacity of

https://doi.org/10.1021/acs.energyfuels.1c00795
Energy Fuels 2021, 35, 10227−10240

the activated carbons is very low and does not exceed 0.31 wt %. The hydrogen storage capacities of the prepared activated carbons are given in Table 1 together with their textural properties. These values were obtained at the maximum working pressure (47 bar). Therefore, it can be said that since there is no compression contribution at room temperature, hydrogen is simply stored by the physical sorption process. Fierro et al. (2010) showed that compression contribution occurs when the pressure applied at room temperature is only above 300 bar.[49] The above results shows that experiments should be carried out at either very low temperatures or high pressures to increase the hydrogen storage capacity.

3.6.2. Hydrogen Storage at Cryogenic Temperature. The interactions that keep hydrogen molecules together become more important at high pressures and cryogenic temperature. Figure 11a–c shows the adsorption isotherms of hydrogen on activated carbons between 0 and 47 bar at 77 K. The adsorption isotherm curves indicate an initial steep increase in the hydrogen uptake at low pressures, an almost horizontal plateau at high pressures, and then decreasing at higher pressures. The rapid increase in hydrogen adsorption at low pressures in the isotherm curves and the subsequent unchanging of the adsorbed amount with increasing pressure is a characteristic feature of monolayer adsorption observed on microporous adsorbents.[50] At 77 K, the strength of the interaction between single layers is very weak at temperatures above the critical temperature of hydrogen.[51] Figure 11 shows the isotherm curves obtained for hydrogen adsorption on the surface of activated carbons produced under different conditions. It is seen from the curves that the hydrogen storage capacities of activated carbons produced with increasing microwave irradiation times, powers, and agent ratios increased. This increase may be due to the highly developed pore structure of activated carbon and its higher BET surface area. In this case, there are more active sites on activated carbons for H_2 adsorption. The maximum hydrogen storage capacity of AC600 at 77 K is 2.53 wt %. It can be said that this value is a remarkable amount, especially when compared to the hydrogen storage capacity of porous adsorbents given in Table 2. These adsorbents are costly and nonsustainable, and their manufacturing processes are not reproducible.[28] AC600 has performed similar or better than nanoporous adsorbents with a higher specific surface area. This shows that the surface area is not the only parameter that needs to be regarded. Many researchers emphasized that hydrogen adsorption at 77 K and sub-atmospheric pressures was governed by the micropore volume and specific surface area of the adsorbent.[52,53] The pore size is also a key factor that governs cryogenic H_2 adsorption under certain pressure conditions. This result justifies previous works that stated the existence of an optimum pore size for H_2 adsorption.[54,55] At higher pressures, all adsorption sites on the surface of AC600 are more fully saturated by hydrogen molecules. The hydrogen storage capacity of activated carbon at 27 bar reaches 2.53 wt %. The high pressure excess adsorption isotherm curves at 77 K for AC600 and other activated carbon samples are shown in Figure 11. With increasing test pressure, excess adsorption reaches a maximum value and then gradually decreases. Theoretically, when gas densities in pore and bulk gas increase at the same rate with respect to pressure, excess adsorption will reach a maximum value. Consequently, the continuous increase in pressure negatively affects the adsorbed amount of hydrogen. At pressures above the critical point of hydrogen,

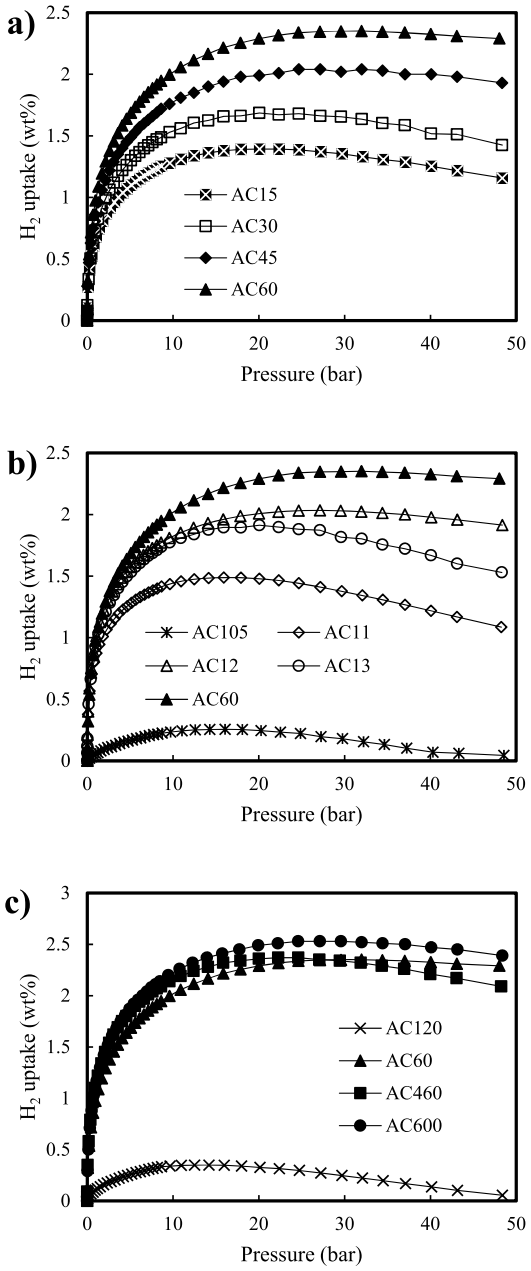

Figure 11. Hydrogen adsorption isotherms of activated carbons at 77 K (a) in different microwave times, (b) in different agent ratios, and (c) in different microwave irradition powers.

the bulk gas density continues to increase while the gas density in the pores of the sample remains unchanged. This case causes the excess adsorption of hydrogen to decrease.[28] Table 2 also shows the hydrogen adsorption data for activated carbons produced from different sources. It can be seen that the activated carbons produced from almond shells possessed similar hydrogen storage capacity with activated carbons produced from other biomass wastes.

The adsorption isotherm gives qualitative information on the adsorption mechanism and porosity of carbonaceous adsorbents.[21] Figure 12 shows the adsorption–desorption isotherm curves of the AC60 sample as a function of pressure at cryogenic temperature. The adsorption–desorption isotherm features an intermediate between types I and II of the International Union of Pure and Applied Chemistry classi-

https://doi.org/10.1021/acs.energyfuels.1c00795
Energy Fuels 2021, 35, 10227–10240

Table 2. Comparison of Physical Properties and Hydrogen Uptake Capacities of the Activated Carbons Prepared from Biomass

	surface properties			H_2 storage			
materials	S_{BET} (m^2/g)	V_t (cc/g)	V_{mic} (cc/g)	Max. (%)	T (K)	P (bar)	references
olive bagasse	1185	0.52	0.43	1.69	77	1	28
				2.59	77	25	
				3.34	77	200	
				0.63	298	200	
empty fruit bunch	687	0.36	0.29	1.97	77	20	30
tangerine peel	1230			1.67	77	30	2
corn cob	3012	1.7	0.98	2	77	1	56
				0.44	298	50	
rice husk	3044	2.25	0.78	2.78	77	1	29
almond shell	1307	1.66	0.7	2.53	77	27	in this study

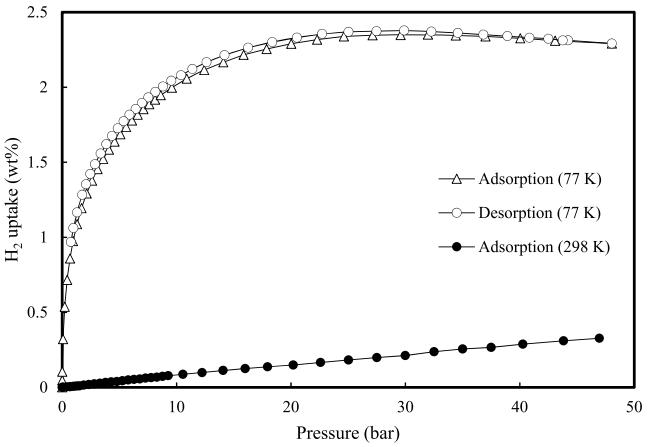

Figure 12. Hydrogen adsorption−desorption isotherm curves of the AC60 sample at cryogenic temperature.

fication, demonstrating that there were micropores with a considerable development of mesoporosity in the activated carbon. Also, Figure 12 shows the hydrogen adsorption capacities of AC60. The hydrogen storage capacity of AC60 at cryogenic temperature is approximately seven times higher than that at room temperature.

The hydrogen adsorption capacities of different carbon nanostructures at 77 and 298 K are related to their specific surface area. The relationship between the maximum hydrogen uptake capacity of activated carbons at room and cryogenic temperatures and their surface areas and micropore volumes was also investigated (Figure 13). Hydrogen adsorption capacity increases with increasing specific surface area and the micropore volume. As a result of the calculations, it was determined that the amount of hydrogen adsorption was highly correlated with both BET surface areas and micropore volumes. It has also been stated in the literature that hydrogen storage capacities are related to BET surface areas or pore volumes, but they do not always have a completely linear relationship.[57]

3.7. Isotherm Analysis. Adsorption isotherms for microporous adsorbents should contain a minimum number of parameters that can interpret the physical properties of the

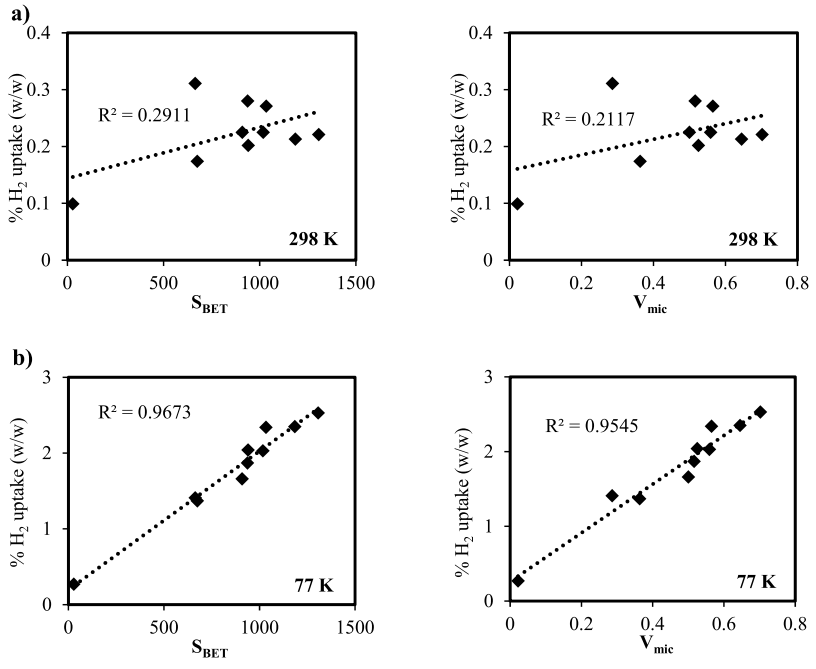

Figure 13. Correlations between the maximum H_2 uptake and BET surface area and micropore volume at (a) 298 K and (b) 77 K.

https://doi.org/10.1021/acs.energyfuels.1c00795
Energy Fuels 2021, 35, 10227−10240

Table 3. Adsorption Isotherm Model Parameters for Hydrogen Adsorption on Activated Carbons

		Freundlich				Langmuir	dual Langmuir	Temkin
samples	Temp. (K)	n_F	K_F (mmol/g)	R^2	ΔH_m (kJ/mol)	R^2	R^2	R^2
AC15	298	0.90	0.002	0.9907	2.2	0.0514	0.1837	0.6544
	77	2.74	0.275	0.9632	1.8	0.9951	0.9749	0.9447
AC30	298	1.06	0.003	0.9919	2.6	0.1975	0.5211	0.5162
	77	2.26	0.313	0.9640	1.5	0.9933	0.9933	0.9317
AC45	298	1.45	0.006	0.9535	3.6	0.5365	0.7541	0.5752
	77	2.70	0.403	0.8342	1.7	0.9941	0.9941	0.8305
AC60	298	0.89	0.003	0.9924	2.2	0.1169	0.2706	0.5284
	77	2.46	0.358	0.9441	1.6	0.9956	0.8775	0.9463
AC105	298	0.81	0.001	0.9627	0.5	0.0782	0.2252	0.6265
	77	1.58	0.042	0.9898	1.0	0.9672	0.4352	0.8557
AC11	298	1.07	0.004	0.9706	2.7	0.0041	0.5495	0.5463
	77	2.76	0.274	0.9407	1.8	0.9962	0.9625	0.9767
AC12	298	0.97	0.003	0.9806	2.4	0.0556	0.5075	0.4036
	77	4.21	0.896	0.9653	2.7	0.9964	0.9964	0.9675
AC13	298	0.98	0.003	0.9734	2.4	0.1077	0.5743	0.4994
	77	2.64	0.336	0.9769	1.7	0.9916	0.9916	0.9392
AC120	298	1.02	0.002	0.9689	2.5	0.0064	0.4201	0.4947
	77	1.88	0.052	0.9934	1.2	0.9758	0.9758	0.8399
AC460	298	1.11	0.002	0.9762	2.8	0.0090	0.6225	0.5846
	77	2.32	0.424	0.9292	1.5	0.9953	0.9953	0.9629
AC600	298	1.54	0.008	0.9463	3.8	0.6297	0.7048	0.6061
	77	2.34	0.467	0.9433	1.5	0.9958	0.9958	0.9436

system. It must also estimate the high pressure maximum observed under supercritical conditions.[58] In this study, the data obtained from hydrogen adsorption isotherm curves were analyzed using Langmuir, Temkin, and Freundlich adsorption isotherm models.

The Langmuir isotherm defines monolayer adsorption in microporous adsorbents. This isotherm assumes that the adsorption energy is constant over all sites on the adsorbent surface, that the adsorption on the surface is localized, and that each site can contain only one atom or molecule. The linear shape of the Langmuir isotherm can be given by the following equation:

$$\frac{P}{n} = \frac{1}{K_1 n_{m1}} + \frac{P}{n_{m1}} \tag{2}$$

where n is the density of adsorption at a pressure of P, n_{m1} is the saturated adsorption value, and K_1 is an equilibrium coefficient.[58] Similarly, a dual Langmuir equation, where each hydrogen molecule dissociates and occupies two sites, can be given as follows:

$$\frac{P^{1/2}}{n} = \frac{1}{K_2 n_{m2}} + \frac{P^{1/2}}{n_{m2}} \tag{3}$$

Note that the monolayer capacity n_{m2} and equilibrium coefficient K_2 have different numerical values in the equation 2 and equation 3 models and thus have been, respectively, subscripted.[59]

The Temkin isotherm contains a parameter that takes into account the adsorbent−adsorbate interactions. It assumes a linear variation of the adsorption heat with the degree of overlap. This equation can be written as follows:

$$n = n_m \frac{RT}{\Delta H_{ads}{}^0 \lambda} \ln(P) + n_m \left(\frac{RT}{\Delta H_{ads}{}^0} \ln K_0 + \frac{1}{\lambda} \right) = A \ln P + B \tag{4}$$

where λ is the proportional decay constant, $\Delta H_{ads}{}^0$ is the standard enthalpy of adsorption, T is the temperature, and R is the ideal gas constant. The constant regression terms are simply $A = n_m \frac{RT}{\Delta H_{ads}{}^0 \lambda}$ and $B = n_m \left(\frac{RT}{\Delta H_{ads}{}^0 \lambda} \ln K_0 + \frac{1}{\lambda} \right)$. The primary weakness of the Temkin model is failure at the low and high pressure extremes due the logarithmic dependence.[60,61]

In contrast to the Temkin model, the Freundlich model attempts to account for surface heterogeneity with a logarithmic energy distribution function. Adsorbed molecules react with each other. The Freundlich isotherm can be given as follows:

$$n = n_m K_0^{(RT)/\Delta H_m} P^{(RT)/\Delta H_m} = K_F P^{1/n_F} \tag{5}$$

in logaritmic form,

$$\ln(n) = \ln(K_F) + \frac{1}{n_F} \ln(P) \tag{6}$$

where K_F is the Freundlich isotherm constant and n_F is the adsorption intensity.[60]

The critical temperature of hydrogen is 32.98 K.[3,58] This means that hydrogen may not condense in the micropores and mesopores of the solid adsorbent at 77 K. In this case, the hydrogen molecules can be physically adsorbed on the surface of the adsorbent. Adsorption isotherm data were fitted with Langmuir, Temkin, and Freundlich adsorption models. The regression coefficient values calculated for these adsorption isotherm models were given in Table 3. From the regression coefficients, it is seen that the Freundlich adsorption model has very good agreement with experimental data at room and

https://doi.org/10.1021/acs.energyfuels.1c00795
Energy Fuels 2021, 35, 10227−10240

cryogenic temperatures. In Table 3, the regression coefficients calculated for the Langmuir isotherm at cryogenic temperature are quite high. However, the experimentally determined maximum hydrogen removal does not match the values calculated from the Langmuir model. For example, the maximum hydrogen removed determined at 77 K for AC60 is 2.34 wt %, while the calculated value from the Langmuir isotherm is 1.11 wt %. This result shows that although the isotherm data at cryogenic temperatures are compatible with the Langmuir model, the experimental and calculated values do not match. Regression coefficients calculated for Temkin models are lower than those of the Freundlich isotherm. These results show that the experimental data fit better with the Freundlich isotherm. As a result, it can be said that the active sites on the activated carbon are not homogeneously distributed and adsorption is not limited to a monolayer.

From the Freundlich equation,

$$\frac{RT}{\Delta H_m} = \frac{1}{n_F} \tag{7}$$

can be written. In this equation, R is the ideal gas constant (J/mol K); T is the temperature (K); and ΔH is the adsorption heat (J/mol). ΔH values were found in a range of 1.0−3.6 kJ/mol. These values show that hydrogen adsorption is a physical adsorption on activated carbon surfaces. Similar results were found by Melouki et al. (2017) in a range of 4.4−5.2 kJ/mol for the adsorption of hydrogen on activated carbon produced from olive waste;[61] Kojima et al. (2006) in a range of 5.5−5.8 kJ/mol for the adsorption of hydrogen on different carbon nanostructures;[43] and Bader and Abdelmottaleb (2017) in a range of 3.5−4.0 kJ/mol for activated carbon produced from olive bagasse by carbon dioxide activation.[28]

4. CONCLUSIONS

In this study, the microwave irradiation method was used to save energy and time in the preparation of activated carbon. In this way, almond shells, which are agricultural wastes, were brought to the industry. Activated carbons were prepared under different experimental conditions and the effects of these conditions on the textural properties of activated carbons were examined. It was found that with increasing microwave irradiation time, power, and agent ratio, the surface areas and total pore volumes of the activated carbons increased. N_2-sorption, FTIR, and SEM results showed that microwave irradiation time, power, and agent ratio significantly affected the morphological, structural, and porosity properties of activated carbons. Considering the hydrogen uptake capacities of activated carbons, the highest value was obtained for AC600 with 2.53 wt % at 77 K and 27 bar. According to FAO data, the total production of almond shells in the world in 2017 is 2,239,697 tons. USA ranks first with a production of 1,029,655 tons and Turkey ranks fifth with a production of 90,000 tons.[62] The shell ratio of the total fruit varies between 35 and 75%, depending on the type of almond.[63] This also shows that almond shells between 783,894 and 1,679,773 tons are released annually. In our study, activated carbon was produced from almond shells with a yield of 26%. This result shows that approximately 203,812−436,741 tons of activated carbon can be produced from the almond shell per year. The contribution of this to the world economy is approximately 20,381,200−43,674,100 Euros. Furthermore, in our study, we determined that 2.53 wt % hydrogen per AC600 gram can be adsorbed. In this case, it can be said that approximately 5156−11,050 tons of hydrogen can be stored by using all activated carbons produced. In addition, the hydrogen adsorption capacity of activated carbons at cryogenic temperature was higher than that at room temperature. This finding showed that the van der Waals interactions between activated carbon and hydrogen increased. The study results indicate that activated carbons prepared from almond shells with less energy and time are suitable for storing hydrogen gas.

AUTHOR INFORMATION

Corresponding Author

Mehmet Doğan − *Faculty of Science and Literature, Department of Chemistry, Balikesir University, Balikesir 10145, Turkey*; orcid.org/0000-0002-3707-0497; Email: mdogan@balikesir.edu.tr, mdogan7979@gmail.com

Author

Zeynep Bicil − *Science and Technology Application and Research Center, Balikesir University, Balikesir 10145, Turkey*

Complete contact information is available at: https://pubs.acs.org/10.1021/acs.energyfuels.1c00795

Notes

The authors declare no competing financial interest.

ACKNOWLEDGMENTS

This work was supported by Balikesir University Office of Scientific Research Projects Coordination [2017/078].

REFERENCES

(1) *The Intergovernmental Panel on Climate Change, Special Report: Global Warming of 1.5°C*; https://www.ipcc.ch/sr15/> (accessed 27 December 2020).

(2) Doğan, M.; Sabaz, P.; Bicil, Z.; Kizilduman, B. K.; Turhan, Y. Activated carbon synthesis from tangerine peel and its use in hydrogen storage. *J. Energy Inst.* **2020**, *93*, 2176−2185.

(3) Guo, H.; Gao, Q. Cryogenic hydrogen uptake of high surface area porous carbon materials activated by potassium hydroxide. *Int. J. Hydrogen Energy* **2010**, *35*, 7547−7554.

(4) Fakioğlu, E.; Yürüm, Y.; Veziroğlu, T. N. A review of hydrogen storage systems based on boron and its compounds. *Int. J. Hydrogen Energy* **2004**, *29*, 1371−1376.

(5) Jiménez, V.; Ramírez-Lucas, A.; Sánchez, P.; Valverde, J. L.; Romero, A. Hydrogen storage in different carbon materials: Influence of the porosity development by chemical activation. *Appl. Surf. Sci.* **2012**, *258*, 2498−2509.

(6) Yürüm, Y.; Taralp, A.; Veziroglu, T. N. Storage of hydrogen in nanostructured carbon materials. *Int. J. Hydrogen Energy* **2009**, *34*, 3784−3798.

(7) Doğan, E. E.; Tokcan, P.; Kizilduman, B. K. Storage of hydrogen in activated carbons and carbon nanotubes. *Adv. Mater. Sci.* **2018**, *18*, 5−16.

(8) Świerczyńska, A.; Fydrych, D.; Landowski, M.; Rogalski, G.; Łabanowski, J. Hydrogen embrittlement of X2CrNiMoCuN25-6-3 super duplex stainless steel welded joints under cathodic protection. *Constr. Build. Mater.* **2020**, *238*, 117697.

(9) Dincer, I. Technical, environmental and exergetic aspects of hydrogen energy systems. *Int. J. Hydrogen Energy* **2002**, *27*, 265−285.

(10) Lindblom, U. E. A conceptual design for compressed hydrogen storage in mined caverns. *Int. J. Hydrogen Energy* **1985**, *10*, 667−675.

(11) Nguyen, M. C.; Lee, H.; Ihm, J. Hydrogen storage using functionalized saturated hydrocarbons. *Solid State Commun.* **2008**, *147*, 419−422.
(12) Sakintuna, B.; Lamari-Darkrim, F.; Hirscher, M. Metal hydride materials for solid hydrogen storage: a review. *Int. J. Hydrogen Energy* **2007**, *32*, 1121−1140.
(13) Hwang, J. Y.; Lee, S. H.; Sim, K. S.; Kim, J. W. Synthesis and hydrogen storage of carbon nanofibers. *Synth. Met.* **2002**, *126*, 81−85.
(14) Zubizarreta, L.; Menéndez, J. A.; Pis, J. J.; Arenillas, A. Improving hydrogen storage in Ni-doped carbon nanospheres. *Int. J. Hydrogen Energy* **2009**, *34*, 3070−3076.
(15) Hayashi, J.; Horikawa, T.; Takeda, I.; Muroyama, K.; Ani, F. N. Preparing activated carbon from various nutshells by chemical activation with K_2CO_3. *Carbon* **2002**, *40*, 2381−2386.
(16) Heidarinejad, Z.; Dehghani, M. H.; Heidari, M.; Javedan, G.; Ali, I.; Sillanpää, M. Methods for preparation and activation of activated carbon: a review. *Environ. Chem. Lett.* **2020**, *18*, 393−415.
(17) Ao, W.; Fu, J.; Mao, X.; Kang, Q.; Ran, C.; Liu, Y.; et al. Microwave assisted preparation of activated carbon from biomass: A review. *Renewable Sustainable Energy Rev.* **2018**, *92*, 958−979.
(18) Alslaibi, T. M.; Abustan, I.; Ahmad, M. A.; Foul, A. A. A review: production of activated carbon from agricultural byproducts via conventional and microwave heating. *J. Chem. Technol. Biotechnol.* **2013**, *88*, 1183−1190.
(19) Norman, L. M.; Cha, C. Y. Production of activated carbon from coal chars using microwave energy. *Chem. Eng. Commun.* **1995**, *140*, 87−110.
(20) Zhong, Z.-Y.; Yang, Q.; Li, X.-M.; Luo, K.; Liu, Y.; Zeng, G.-M. Preparation of peanut hull-based activated carbon by microwave-induced phosphoric acid activation and its application in Remazol Brilliant Blue R adsorption. *Ind. Crops. Prod.* **2012**, *37*, 178−185.
(21) Yang, K.; Peng, J.; Srinivasakannan, C.; Zhang, L.; Xia, H.; Duan, X. Preparation of high surface area activated carbon from coconut shells using microwave heating. *Bioresour. Technol.* **2010**, *101*, 6163−6169.
(22) Deng, H.; Yang, L.; Tao, G.; Dai, J. Preparation and characterization of activated carbon from cotton stalk by microwave assisted chemical activation—application in methylene blue adsorption from aqueous solution. *J. Hazard. Mater.* **2009**, *166*, 1514−1521.
(23) Liu, Q.-S.; Zheng, T.; Wang, P.; Guo, L. Preparation and characterization of activated carbon from bamboo by microwave-induced phosphoric acid activation. *Ind. Crops Prod.* **2010**, *31*, 233−238.
(24) Yagmur, E.; Ozmak, M.; Aktas, Z. A novel method for production of activated carbon from waste tea by chemical activation with microwave energy. *Fuel* **2008**, *87*, 3278−3285.
(25) Foo, K. Y.; Hameed, B. H. Preparation, characterization and evaluation of adsorptive properties of orange peel based activated carbon via microwave induced K_2CO_3 activation. *Bioresour. Technol.* **2012**, *104*, 679−686.
(26) Li, G.; Li, J.; Tan, W.; Jin, H.; Yang, H.; Peng, J.; et al. Preparation and characterization of the hydrogen storage activated carbon from coffee shell by microwave irradiation and KOH activation. *Int. Biodeterior. Biodegrad.* **2016**, *113*, 386−390.
(27) Yu, F.; Steele, P. H.; Ruan, R. Microwave pyrolysis of corn cob and characteristics of the pyrolytic chars. *Energy Sources, Part A* **2010**, *32*, 475−484.
(28) Bader, N.; Abdelmottaleb, O. CO_2 activation of olive bagasse for hydrogen storage. *Environ. Prog. Sustainable Energy* **2017**, *36*, 315−324.
(29) Heo, Y.-J.; Park, S.-J. Synthesis of activated carbon derived from rice husks for improving hydrogen storage capacity. *J. Ind. Eng. Chem.* **2015**, *31*, 330−334.
(30) Ramesh, T.; Rajalakshmi, N.; Dhathathreyan, K. S. Activated carbons derived from tamarind seeds for hydrogen storage. *J. Energy Storage* **2015**, *4*, 89−95.
(31) Hasar, H. Adsorption of nickel (II) from aqueous solution onto activated carbon prepared from almond husk. *J. Hazard. Mater.* **2003**, *97*, 49−57.
(32) Ahsaine, H. A.; Zbair, M.; Anfar, Z.; Naciri, Y.; El Haouti, R.; El Alem, N.; Ezahri, M. Cationic dyes adsorption onto high surface area 'almond shell'activated carbon: kinetics, equilibrium isotherms and surface statistical modeling. *Mater. Today Chem.* **2018**, *8*, 121−132.
(33) Pragya, P. Preparation and study of properties of activated carbon produced from agricultural and industrial waste shells. *Res. J. Chem. Sci.* **2013**, *3*, 12−15.
(34) İzgi, M. S.; Saka, C.; Baytar, O.; Saraçoğlu, G.; Şahin, Ö. Preparation and characterization of activated carbon from microwave and conventional heated almond shells using phosphoric acid activation. *Anal. Lett.* **2019**, *52*, 772−789.
(35) Du, C.; Yang, H.; Wu, Z.; Ge, X.; Cravotto, G.; Ye, B. C.; Kaleem, I. Microwave-assisted preparation of almond shell-based activated carbon for methylene blue adsorption. *Green Processes Synth.* **2016**, *5*, 395−406.
(36) Doğan, M.; Alkan, M.; Çakir, Ü. Electrokinetic properties of perlite. *J. Colloid Interface Sci.* **1997**, *192*, 114−118.
(37) Alkan, M.; Demirbaş, Ö.; Doğan, M. Zeta potential of unexpanded and expanded perlite samples in various electrolyte media. *Microporous Mesoporous Mater.* **2005**, *84*, 192−200.
(38) Hesas, R. H.; Daud, W. M. A. W.; Sahu, J. N.; Arami-Niya, A. The effects of a microwave heating method on the production of activated carbon from agricultural waste: A review. *J. Anal. Appl. Pyrolysis* **2013**, *100*, 1−11.
(39) Gao, Q.; Liu, H.; Cheng, C.; Li, K.; Zhang, J.; Zhang, C.; Li, Y. Preparation and characterization of activated carbon from wool waste and the comparison of muffle furnace and microwave heating methods. *Powder Technol.* **2013**, *249*, 234−240.
(40) Foo, K. Y.; Hameed, B. H. Porous structure and adsorptive properties of pineapple peel based activated carbons prepared via microwave assisted KOH and K_2CO_3 activation. *Microporous Mesoporous Mater.* **2012**, *148*, 191−195.
(41) Lua, A. C.; Yang, T. Characteristics of activated carbon prepared from pistachio-nut shell by zinc chloride activation under nitrogen and vacuum conditions. *J. Colloid Interface Sci.* **2005**, *290*, 505−513.
(42) Strezov, V.; Moghtaderi, B.; Lucas, J. A. Thermal study of decomposition of selected biomass samples. *J. Therm. Anal. Calorim.* **2003**, *72*, 1041−1048.
(43) Kojima, Y.; Kawai, Y.; Koiwai, A.; Suzuki, N.; Haga, T.; Hioki, T.; Tange, K. Hydrogen adsorption and desorption by carbon materials. *J. Alloys Compd.* **2006**, *421*, 204−208.
(44) Peredo-Mancilla, D.; Ghouma, I.; Hort, C.; Bessieres, D.; Ghimbeu, C. M. *Char and Carbon Materials Derived from Biomass*; Jeguirim, M.; Limousy, L. (Eds.), Elsevier: 2019, pp. 341−382.
(45) Banerjee, S.; Murad, S.; Puri, I. K. Hydrogen storage in carbon nanostructures: possibilities and challenges for fundamental molecular simulations. *Proc. IEEE* **2006**, *94*, 1806−1814.
(46) Yoo, E.; Gao, L.; Komatsu, T.; Yagai, N.; Arai, K.; Yamazaki, T.; et al. Atomic hydrogen storage in carbon nanotubes promoted by metal catalysts. *J. Phys. Chem. B* **2004**, *108*, 18903−18907.
(47) Blackman, J. M. High pressure hydrogen storage on carbon materials for mobile applications. PhD Thesis. University of Nottingham; 2005.
(48) Züttel, A.; Borgschulte, A.; Schlapbach, L. *Hydrogen as a Future Energy Carrier*; 1st ed., Wiley-VCH: Weinheim, 2008
(49) Fierro, V.; Zhao, W.; Izquierdo, M. T.; Aylon, E.; Celzard, A. Adsorption and compression contributions to hydrogen storage in activated anthracites. *Int. J. Hydrogen Energy* **2010**, *35*, 9038−9045.
(50) Lowell, S.; Shields, J. E. *Powder Surface Area and Porosity*; 3rd ed., Springer Science & Business Media: 1991
(51) Hirscher, M. *Handbook of hydrogen storage: new materials for future energy storage*; 1st ed., John Wiley & Sons: 2010
(52) Wang, H.; Gao, Q.; Hu, J. High hydrogen storage capacity of porous carbons prepared by using activated carbon. *J. Am. Chem. Soc.* **2009**, *131*, 7016−7022.
(53) Kunowsky, M.; Marco-Lozar, J. P.; Oya, A.; Linares-Solano, A. Hydrogen storage in CO_2-activated amorphous nanofibers and their monoliths. *Carbon* **2012**, *50*, 1407−1416.

https://doi.org/10.1021/acs.energyfuels.1c00795
Energy Fuels 2021, 35, 10227−10240

(54) Celzard, A.; Fierro, V.; Marêché, J. F.; Furdin, G. Advanced preparative strategies for activated carbons designed for the adsorptive storage of hydrogen. *Adsorpt. Sci. Technol.* **2007**, *25*, 129−142.
(55) Georgiev, P. A.; Ross, D. K.; Albers, P.; Ramirez-Cuesta, A. J. The rotational and translational dynamics of molecular hydrogen physisorbed in activated carbon: a direct probe of microporosity and hydrogen storage performance. *Carbon* **2006**, *44*, 2724−2738.
(56) Sun, Y.; Webley, P. A. Preparation of activated carbons from corncob with large specific surface area by a variety of chemical activators and their application in gas storage. *Chem. Eng. J.* **2010**, *162*, 883−892.
(57) Zhang, C.; Geng, Z.; Cai, M.; Zhang, J.; Liu, X.; Xin, H.; Ma, J. Microstructure regulation of super activated carbon from biomass source corncob with enhanced hydrogen uptake. *Int. J. Hydrogen Energy* **2013**, *38*, 9243−9250.
(58) Bénard, P.; Chahine, R. Determination of the adsorption isotherms of hydrogen on activated carbons above the critical temperature of the adsorbate over wide temperature and pressure ranges. *Langmuir* **2001**, *17*, 1950−1955.
(59) Lam, S. T.; Ballinger, R.; Forsberg, C. Modeling and predicting total hydrogen adsorption in nanoporous carbon materials for advanced nuclear systems. *J. Nucl. Mater.* **2018**, *511*, 328−340.
(60) Temkin, M. I. Adsorption equilibrium and the kinetics of processes on nonhomogeneous surfaces and in the interaction between adsorbed molecules. *Zh. Fiz. Chim.* **1941**, *15*, 296−332.
(61) Melouki, R.; Llewellyn, P. L.; Tazibet, S.; Boucheffa, Y. Hydrogen adsorption on activated carbons prepared from olive waste: effect of activation conditions on uptakes and adsorption energies. *J. Porous Mater.* **2017**, *24*, 1−11.
(62) Gok, S.; Aka Kacar, Y.; Kuden, A. A General View to Almond Breeding Studies in the World and Turkey. *Çukurova J. Agric. Food Sci.* **2020**, *35*, 67−76.
(63) Ebringerová, A.; Hromádková, Z.; Košťálová, Z.; Sasinková, V. Chemical valorization of agricultural by-products: isolation and characterization of xylan-based antioxidants from almond shell biomass. *BioResources* **2008**, *3*, 60−70.

https://doi.org/10.1021/acs.energyfuels.1c00795
Energy Fuels 2021, 35, 10227−10240